Structure formation in perfluoropentacene:diindenoperylene blends and its impact on transient effects in the optical properties studied in real-time during growth

K. Broch,[1] A. Gerlach,[1,a)] C. Lorch,[1] J. Dieterle,[1] J. Novák,[1] A. Hinderhofer,[1,2] and F. Schreiber[1]

[1]*Universität Tübingen, Institut für Angewandte Physik and LISA+, Auf der Morgenstelle 10, 72076 Tübingen, Germany*
[2]*Graduate School of Advanced Integration Science, Chiba University, 1-33 Yayoi-cho, Inage-ku, Chiba 263-8522, Japan*

We discuss the result of the competing effects of favourable intermolecular interactions and steric incompatibilities due to the size mismatch of perfluoropentacene (PFP) and diindenoperylene (DIP) on the structure formation and associated optical properties in mixed films. Using real-time grazing incidence X-ray diffraction we investigate the size of coherently scattering islands l_s as a function of film thickness and mixing ratio. We find that for PFP:DIP 1:2 blends l_s is by a factor of $\sim$4 smaller than in pure DIP films, while l_s of the PFP:DIP 2:1 blends is not significantly reduced compared with pure PFP. Yet, we observe an increase in l_s with film thickness for all of the samples, independent on the mixing ratio. In parallel with the structural characterization we investigate the evolution of the absorption spectra in the visible spectral range and its dependence on l_s *in situ* during film growth using differential reflectance spectroscopy. We observe a surprisingly strong effect of changes in the structural order on the shape of $\epsilon_{2,xy}(E)$, evident by a pronounced evolution of characteristic peaks in the thickness range from 1.6 nm to 9.6 nm. The combined results of the real-time experiments allow to identify the thickness dependent crystal grain size as the origin of the observed transient effects in the absorption spectra. © 2013 AIP Publishing LLC. [http://dx.doi.org/10.1063/1.4827868]

I. INTRODUCTION

Binary mixtures of organic semiconductors are not only relevant for device applications,[1–9] but also pose fundamental questions regarding their growth behavior and the associated optical properties. The structural properties of these systems are influenced by different effects, such as intermolecular interactions and steric properties of the compounds, which affect the mixing (i.e., phase separation vs. intermixing)[10] as well as the crystalline ordering behavior.[11] The optical and electronic properties of the system can depend strongly on the film structure[12–17] and investigations of the underlying mechanisms of structure formation and ordering behavior are necessary for a detailed understanding of these phenomena.[18,19] Importantly, the resulting post growth structure does not always allow to deduce these mechanisms. Growth is a dynamic phenomenon, and transient effects in structural order as well as in the optical properties[20] may occur and have to be investigated *in situ* and in real-time.[21–24] Apart from the film structure, also intermolecular coupling can significantly affect the optical properties of the mixed system either due to the differences in the film structure compared with the pure films, which results in changes in the intermolecular interactions between molecules of the same compound,[25] or due to a

possible charge transfer between molecules of the two different compounds.[26–31]

Pentacene (PEN, $C_{22}H_{14}$) and diindenoperylene (DIP, $C_{32}H_{16}$) are two of the most prominent small-molecule organic semiconductors,[13,33–36] which exhibit an anomalous ordering in PEN:DIP blends with a smectic-C-like structure.[11] The perfluorinated derivative of PEN (PFP, $C_{22}F_{14}$) has recently attracted significant interest in pure films as well as in blends with PEN.[37–44] It is very tempting to study blends of PFP and DIP as the two compounds exhibit favourable intermolecular interactions, *inter alia* due to their quadrupole moments of opposite sign and are known to form an intermixed crystal phase.[32] Yet, the structure formation during the growth of mixed thin films is possibly influenced by the competition between the favourable intermolecular interaction and the steric incompatibility due to the size mismatch between PFP and DIP. As there is a tight connection of structural and optical properties, the latter may be significantly affected by changes in the film structure or the crystalline order during the growth of the samples. This may not only result in deviations in the shape of the spectra compared with the pure films, but possibly also in a pronounced dependence of the spectral shape on the film thickness d. Using grazing incidence X-ray diffraction (GIXD) and differential reflectance spectroscopy (DRS) we address this effect by following the evolution of coherently scattering islands in the film and $\epsilon_{2,xy}(E)$ (related to the absorption spectrum in

a)Electronic mail: alexander.gerlach@uni-tuebingen.de

the visible spectral range) during film growth *in situ* and in real-time.

II. EXPERIMENTAL

Mixed films of PFP and DIP were grown using organic molecular beam deposition[3,6] in ultra-high vacuum at a constant substrate temperature of 300 K and with different molar mixing ratios of PFP and DIP (4:1, 2:1, 1:1, 1:2, 1:4), which were determined as described in Refs. 26 and 45. Two different series of samples have been prepared. The films of the first series with a film thickness of $d = 22\text{-}25$ nm and five different mixing ratios were used for post growth X-ray reflectivity (XRR)-studies and *in situ* DRS-measurements. For this purpose, the mixed films have been grown at a base pressure of $p = 2 \times 10^{-10}$ mbar simultaneously on two different types of substrates, namely 0.5 mm thick Si(100) substrates with a 2 nm SiO_2-layer (NativeSi) and 0.5 mm thick quartz glass substrates. The XRR data were obtained *ex situ* in air with a GE-Seifert X-ray reflectometer using Cu $K_{\alpha 1}$-radiation ($\lambda = 1.541$ Å) in the range $q_z = 0\text{--}1$ Å^{-1}. DRS-measurements were performed at normal incidence on the quartz glass substrate in the energy range from 1.4 eV to 3.0 eV using a DH-2000 deuterium-tungsten halogen-light source and an USB-2000+ spectrometer of Ocean Optics. Before growth, the backside of the substrate was roughened to avoid backreflections. The DRS-signal is defined as[46–48]

$$\text{DRS} = \frac{R(d) - R_0}{R_0}, \qquad (1)$$

where $R(d)$ corresponds to the reflectivity of the substrate covered with a film with thickness d and R_0 denotes the reflectivity of the bare substrate. The data were analyzed using a Gaussian oscillator model to describe the dielectric function of the material.[20]

A second series of samples consisting of mixed films with three different mixing ratios (PFP:DIP 2:1, 1:1, 1:2) and with film thicknesses from $d = 12$ nm to 16 nm was prepared in a portable UHV-chamber (base pressure $p = 1 \times 10^{-9}$ mbar) using NativeSi as substrate. Real-time GIXD measurements, which are a powerful technique to monitor the thin film growth[49–53] *in situ*, were performed on this series to study the crystallization of PFP:DIP mixtures. The real-time GIXD data were measured at the MS-Surf-Diffraction beamline (Swiss Light Source, Villigen, Switzerland)[54,55] with a wavelength of 0.954 Å in the range $q_{||} = 1.61\text{--}1.99$ Å^{-1} using a Pilatus II-detector with 487×195 pixels.

III. RESULTS

A. Post growth XRR-measurements

The structural properties of equimolar PFP:DIP mixtures determined post growth have been discussed in Ref. 32. For the equimolar mixture no Bragg-peaks at $q_{||}$-positions corresponding to the pure films were observed, but Bragg-peaks significantly different in $q_{||}$-position indicate the formation of a mixed crystal phase. If the mixing ratio was deviating from the equimolar ratio, a coexistence of in-plane Bragg peaks
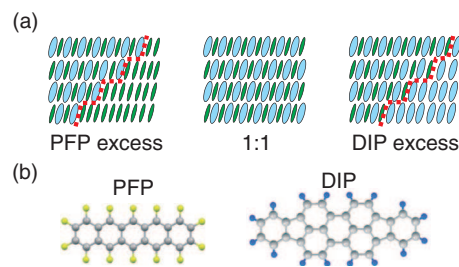
FIG. 1. (a) Schematic mixing scenarios of PFP:DIP blends with different mixing ratios.[32] (b) Sketches of the molecules.

corresponding to the mixed crystal phase and the pure film phase of the excess compound was found. We completed the post growth structural investigations of PFP:DIP blends by XRR-measurements of samples with non-equimolar mixing ratios (see Fig. 2).

The data show that in the equimolar mixed films two types of crystal domains can be distinguished by the molecular orientation: In the first type, the molecules are standing almost upright relative to the substrate (σ-orientation[32]). The second type consists of domains with nearly flat lying molecules and large mosaicity (λ-orientation[32]). The intensity of the Bragg peak corresponding to the λ-orientation changes significantly with the mixing ratio, indicating that the nucleation of domains consisting of molecules in the λ-orientation is facilitated in mixtures containing more PFP.

Similar to the equimolar mixture, also in the XRR data of all non-equimolar mixtures the (100)- and (200)-reflection of the σ-orientation can be observed. Compared to the equimolar mixture the Bragg peak positions are slightly shifted in the mixed films with non-equimolar mixing ratios. Since these blends exhibit a phase coexistence between a mixed and a pure film phase of the excess compound[32] (Fig. 1(a)) the measured Bragg peaks are composed of two Bragg-reflections, one stemming from the mixed film phase and the other one
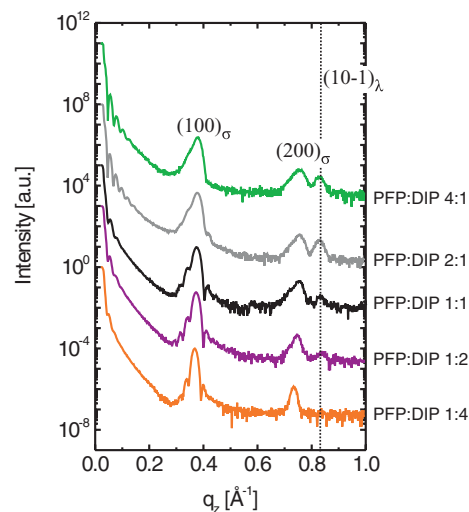
FIG. 2. XRR data of PFP:DIP films with five different mixing ratios (PFP:DIP 4:1, 2:1, 1:1, 1:2, 1:4) and film thicknesses $d = 22\text{–}25$ nm, prepared at a substrate temperature of $T_{\text{sub}} = 300$ K. The data are vertically offset for clarity. The straight line marks the Bragg peak which was assigned to domains of lying molecules.[32]

TABLE I. Roughness σ and mass density ρ_{exp} for PFP and DIP films and the five different PFP:DIP blends, determined by fits of the XRR data presented in Fig. 2. For comparison the calculated mass density ρ_{calc} based on the molecular weight and the unit cell volumes of PFP,[42] DIP,[58] and the equimolar PFP:DIP mixed film phase[32] is noted.

Mixing ratio	σ (nm)	ρ_{exp} (g/cm^3)	ρ_{calc} (g/cm^3)
PFP	4.50	2.10	2.05
PFP:DIP 4:1	2.53	1.74	1.87
PFP:DIP 2:1	2.74	1.63	1.77
PFP:DIP 1:1	3.43	1.51	1.64
PFP:DIP 1:2	3.20	1.38	1.51
PFP:DIP 1:4	3.76	1.34	1.42
DIP	4.88	1.33	1.29

arising from the respective pure film phase, which can lead to a peak shift.[45] Using the program GenX[56] the XRR data were fitted based on the Parratt formalism[57] for low q_z up to $q_z^{max} = 0.16$ Å^{-1}. In order to determine the film thickness d, the roughness σ, and the mass density ρ, a model with three layers (*bulk Si-substrate, SiO$_2$-layer* ($d \approx 1.8$ *nm*), *organic film*) was used. The fit results are compiled in Table I and Fig. 3.

Remarkably, the mixed films are smoother than the pure ones for all mixing ratios. With increasing relative volume fraction of DIP, the roughness as well as the coherently scattering volume of the film increases. A similar smoothing of the films upon mixing was already observed for blends of PFP:PEN[45] and PEN:DIP[11] although a full explanation appears to be still lacking. The mass density ρ_{exp} is decreasing with increasing amount of DIP. This trend is in agreement with the calculated mass densities ρ_{calc} for the various mixtures, which were calculated via

$$\rho_{calc} = \frac{x_{PFP} \cdot \rho_{PFP} + 1.2 x_{DIP} \cdot \rho_{DIP}}{x_{PFP} + 1.2 x_{DIP}}. \quad (2)$$

Here, x_{PFP} (x_{DIP}) is the relative volume fraction of PFP (DIP) and ρ_{PFP} (ρ_{DIP}) is the mass density of PFP (DIP). The factor 1.2 is introduced to correct for the differences in the unit cell volumes of PFP[42] and DIP.[58] As it can be seen in Fig. 3(b), for the PFP:DIP blends ρ_{calc} is larger than ρ_{exp}, in contrast to the pure films, for which both values are in agreement within the error of the fit. The small difference in ρ_{calc} and ρ_{exp} of a few % may be due to the different unit cell volume of the mixed crystal phase from the unit cell volumes of the pure compounds.

B. Real-time *in situ* experiments

1. Real-time GIXD experiments

In order to investigate if and how the different steric properties of PFP and DIP influence the formation of crystallites during film growth we performed real-time GIXD experiments concentrating on the range $q_{\parallel} = 1.61$–1.99 Å^{-1}, where the $\sigma(020)$-reflection of the mixed crystal phase is found. For non-equimolar blends the (012)-reflection of pure PFP or the (120)-reflection of pure DIP is also observed within this q-range.

Figure 4 shows the real-time GIXD data, with the film thickness d increasing linearly with time. The color scale on the right-hand side denotes the intensity. The peaks were fitted with Lorentzians using the program Fityk.[59] The average size l_s of the coherently scattering islands was determined
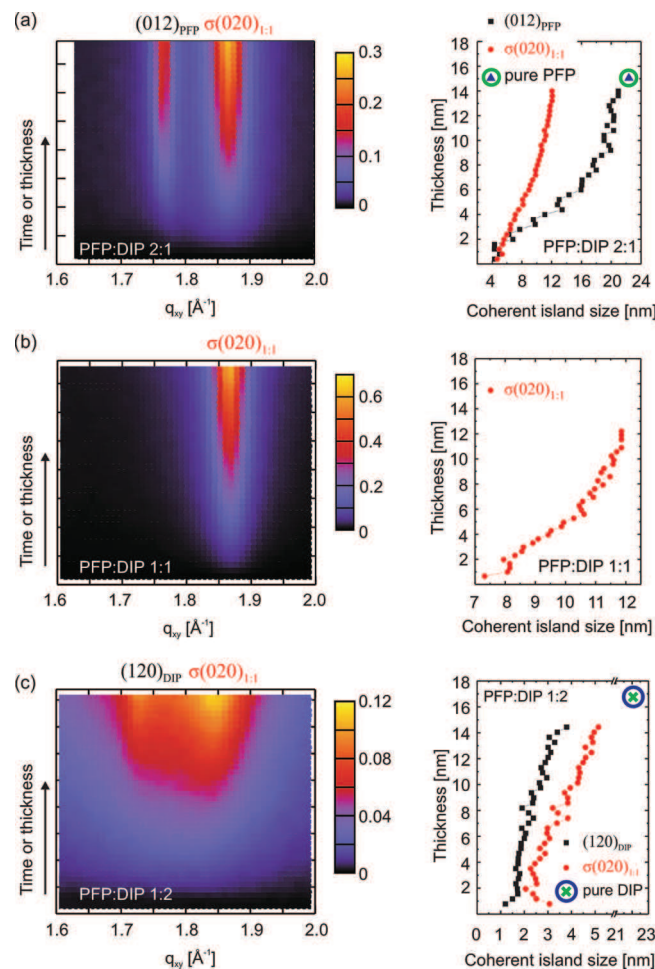
FIG. 4. Real-time GIXD data of PFP:DIP mixtures prepared at a substrate temperature of $T_{sub} = 300$ K, with the film thickness d increasing linearly with time to the final film thickness d_{final}, and the coherently scattering island size l_s as a function of film thickness d. Mixing ratios (a) PFP:DIP 2:1, $d_{final} = 16$ nm, (b) PFP:DIP 1:1, $d_{final} = 12$ nm, and (c) PFP:DIP 1:2, $d_{final} = 14$ nm. For comparison the size of the coherently scattering islands of pure PFP (blue triangle[45]) and pure DIP (green cross) is also shown in (a) and (c), respectively. Note that for higher T_{sub} the island size may be larger.

FIG. 3. (a) Root-mean-square roughness σ, resulting from the fit of the XRR data, and (b) mass density ρ, determined from the fit of the total reflection edge, of PFP:DIP blends as a function of PFP volume fraction, see Table I. The error bars are in the order of the symbol size. For comparison the fit results for the pure films are also shown.
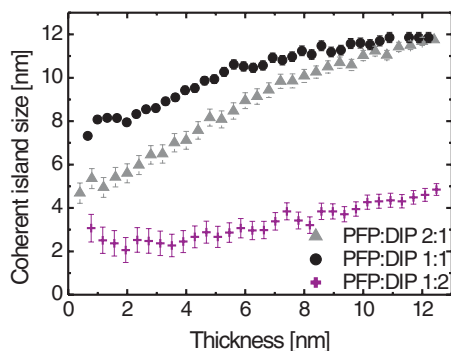
FIG. 5. Comparison of the evolution of l_s of the mixed film phase (see data in Fig. 4) in the different blends. Circles: equimolar mixture, triangles: PFP:DIP 2:1, crosses: PFP:DIP 1:2.

using the Scherrer-formula[60] from the FWHM of the peaks. The evolution of l_s with the film thickness d is shown on the right panels in Fig. 4.

When comparing the l_s-values of the blends with those of the pure films, one finds a pronounced impact of the mixing with another compound on l_s. Note the difference by more than a factor of 4 between the crystallite size in the DIP-phase in the mixture compared to the pure DIP film (Fig. 4(c)). In contrast, the crystallite size in the pure PFP film and the PFP-phase in the mixture is in remarkable agreement (Fig. 4(a)). Apparently, in the PFP:DIP 1:2 blend the nucleation of crystallites of the DIP excess phase is hindered to a greater extent by the nucleation of crystallites of the equimolar mixed crystal phase compared with the PFP excess phase in the PFP:DIP 2:1 blend. Furthermore, we observe differences in the evolution of the crystallite size during growth. In the blend containing more DIP only small crystallites of the DIP excess phase form which do not grow significantly with film thickness (l_s = 1.7 nm for d = 1.5 nm and l_s = 3.8 nm for d = 14.4 nm). For the mixture containing more PFP the crystallite size of the PFP phase is l_s = 4.3 nm in the beginning of growth (d = 1.5 nm) and increases by almost a factor of 5 as the growth proceeds (l_s = 20.9 nm at d = 16 nm).

Similar to the crystallite size of the pure film phases, also the values found for the crystallites of the mixed film phase are influenced by the mixing ratio (Fig. 5). For the PFP:DIP

1:2 blend we observe a $l_s \leq 5$ nm, which is by a factor of 2 smaller compared with l_s for the PFP:DIP 1:1 and PFP:DIP 2:1 blend. Furthermore, l_s of the mixed film phase at the beginning of film growth is largest in the equimolar mixture, indicating that the nucleation of new PFP:DIP-crystallites is hindered by the formation of crystallites of the excess compound in non-equimolar blends. It appears that an excess DIP molecule is more probable to disturb the crystalline order[61] of the stable 1:1 mixed crystal than an excess PFP molecule. Such a surprisingly asymmetric mixing behavior was also observed for a 2D mixture of pentacene and perfluorinated Cu-phthalocyanine.[62]

2. Thickness dependence of the imaginary part of the dielectric function

Complementary to the investigation of the evolution of crystalline order we studied the optical properties of the blends in real-time. We concentrated on the imaginary part ϵ_2 of the dielectric function, which is related to the absorption of the material. PFP:DIP mixtures exhibit uniaxial anisotropy, i.e., their optical properties differ for the direction parallel to the substrate surface (*xy*-direction) and perpendicular to the substrate surface (*z*-direction). Due to the normal incidence geometry DRS probes exclusively $\epsilon_{2,\,xy}(E)$.

The optical properties of equimolar PFP:DIP mixtures measured post growth are reported in Ref. 32. There, also the shift of the first observable peak in $\epsilon_{2,\,xy}(E)$ of the equimolar PFP:DIP mixture with film thickness was discussed. The evolution of the shape of $\epsilon_{2,\,xy}(E)$ with time has not been reported so far and it may be strongly dependent on the film thickness, due to the significant increase of l_s. Figure 6 shows $\epsilon_{2,\,xy}(E)$ at different film thicknesses for three different mixing ratios (PFP:DIP 2:1, 1:1, 1:2). The data are in agreement with post growth ellipsometry data.[25,32] Although the assignment for most of the peaks is not unique, the peaks at 1.8 eV and 2.0 eV can be attributed to PFP, since DIP shows no absorption in this region. For photon energies of 2.2 eV and higher, both DIP and PFP contribute to $\epsilon_{2,\,xy}(E)$.

Figure 7 shows a comparison of the energy shift ΔE for the first peak (see dashed black lines in Figs. 6(a)–6(c)) for the three different mixing ratios. ΔE of the first peak is very
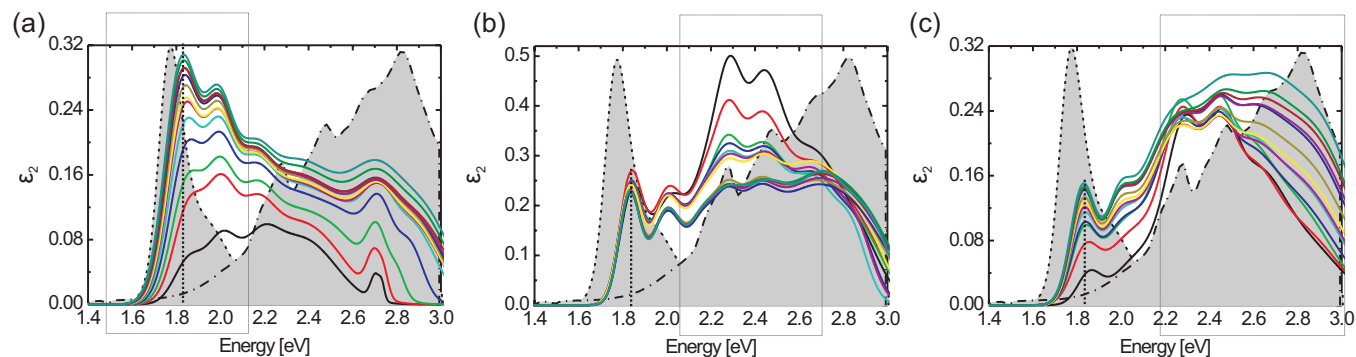
FIG. 6. Real-time evolution of $\epsilon_{2,\,xy}(E)$ for (a) a PFP:DIP 2:1-mixture, (b) a PFP:DIP 1:1-mixture, and (c) a PFP:DIP 1:2-mixture. Each spectrum corresponds to a different film thickness d increasing from d = 1.6 nm (black line) to d = 20.8 nm (green line) in steps of d = 1.6 nm/spectrum. For comparison $\epsilon_{2,\,xy}(E)$ of pure PFP (dotted line) and DIP (dashed-dotted line) are also shown as grey shaded areas. Note that for better comparison the spectra of the pure compounds are scaled by a factor of 0.3 (PFP) and 0.45 (DIP) in (a), (c) and by a factor of 0.45 (PFP) and 0.7 (DIP) in (b).
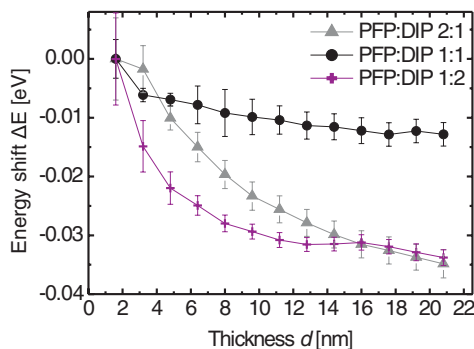
FIG. 7. Energy shift of the first peak corresponding to the lowest electronic transition of PFP (see dashed line in Fig. 6) for the three different mixtures.

small for the equimolar mixture, in remarkable contrast to the energy shift in both non-equimolar blends. The difference in the energy shift may be due to the phase separation between the intermixed crystal phase and a pure phase of the excess compound. Therefore, in non-equimolar blends different effects contribute to the energy shift of the peak: (i) The redshift due to the changing surface-to-bulk ratio with increasing film thickness, which is reported for some pure organic semiconductors.[20,63] (ii) Changes in the local environment for a given molecule in the mixed film phase and the pure film phase of the excess compound during the formation and growth of the crystallites of the two phases. As blends are complex systems also intermolecular interactions between the molecules in the mixed film phase may change during film growth, which may further contribute to changes in the energy position of peaks.

In addition to the energy shift, we observe pronounced changes in the shape of $\epsilon_{2,xy}(E)$ with film thickness for all three systems. In the following we restrict our discussion to spectral ranges where the strongest effects are found, see rectangles in Fig. 6. For the mixture containing more PFP (Fig. 6(a)) the relative intensity of the first two peaks at 1.8 eV and 2.0 eV changes strongly with the film thickness d. While the first peak is weaker than the second peak for low thicknesses, it becomes more intense with increasing thickness, until the shape of $\epsilon_{2,xy}(E)$ resembles that of pure PFP.[39] These two peaks may be assigned to pure PFP and may be interpreted either as the two Davydov components of the transition from the highest occupied molecular orbital (HOMO) to the lowest unoccupied molecular orbital (LUMO) or as the HOMO-LUMO transition and a corresponding vibronic progression.[37,39] Hence, a change in the relative intensities of the two transitions points towards differences in the intermolecular environment and accordingly in the intermolecular interactions during film growth. A possible origin of these changes is the increase in the size of coherently scattering islands of the PFP excess phase, which we observe in the real-time GIXD experiments (see Fig. 4(a)). Indeed, the most pronounced changes in the shape of $\epsilon_{2,xy}(E)$ are found in the thickness range $d = 1.6$–9.6 nm, where l_s increases by a factor of ∼5. Due to the small crystallite size at the beginning of the growth the shape of $\epsilon_{2,xy}(E)$ resembles $\epsilon_2(E)$ of PFP in solution,[39] in particular regarding the relative intensity of the first two peaks. With increasing l_s, and accordingly

improving structural order, the shape of $\epsilon_{2,xy}(E)$ approaches that of pure PFP films. Small differences in the shape of $\epsilon_{2,xy}(E)$ between the mixed and the pure film could be due to the contributions from DIP and the different intermolecular interactions within the intermixed phase.

For the equimolar mixture (Fig. 6(b)) we observe the most pronounced changes in the spectral region from 2.2 eV to 2.6 eV. Here, we have clear indications for a reorientation of the molecules, as two strong peaks decrease significantly in intensity with increasing film thickness. From the comparison with $\epsilon_{2,z}(E)$ of pure DIP, which has strong absorption features in this spectral region,[64] these two peaks can tentatively be assigned to this compound. A possible explanation for the observed change in intensities could be a reorientation of the DIP molecules, as it is reported for pure DIP films.[50] Due to the high intensity of $\epsilon_{2,z}(E)$, which is for DIP much stronger than $\epsilon_{2,xy}(E)$,[64] already a small change in the molecular tilt angle can cause significant changes in the line shape.

Finally, for the blend containing more DIP (Fig. 6(c)) we observe changes in $\epsilon_{2,xy}(E)$ for photon energies of 2.2 eV and above. This is especially interesting, as the peak, which is observed at 2.8 eV, is in pure DIP films an indication for the strength of intermolecular interaction between DIP molecules.[64] With increasing film thickness the relative intensity of the peaks between 2.2 eV and 2.4 eV remains constant, while peaks at 2.6 eV and 2.8 eV are clearly increasing in intensity. This can be rationalized by an increasing intermolecular interaction between DIP molecules with increasing film thickness and increasing in-plane crystallite size l_s. Compared to the pure film spectrum of DIP[20] the peaks are significantly broadened, indicating a lower crystalline order in the film, as confirmed by the low l_s-value determined with GIXD experiments.

For all mixing ratios we find that the size of l_s, which is related to the long-range order within the film, has a pronounced impact on the shape of the absorption spectra. Such a surprisingly clear effect was to the best of our knowledge not reported before.

IV. SUMMARY

The influence of the competition between favourable intermolecular interactions and steric incompatibilities on the film structure and the structure formation in blends of PFP:DIP was investigated post growth as well as in real-time. The nucleation of domains with the two molecular orientations observed in PFP:DIP-blends was found to be strongly influenced by the mixing ratio. While the λ-orientation is very pronounced in blends containing more PFP, the σ-orientation clearly dominates in blends with an excess of DIP. Independent of the mixing ratio the roughness of the mixed films was found to be lower than that of the pure films.

The evolution of l_s with increasing film thickness was studied for the different mixed systems and the effects of increasing size of coherently scattering islands on the shape of $\epsilon_{2,xy}(E)$ were discussed. We observe a significant impact of the limited steric compatibility of the two compounds on the structure formation during growth of the blends. In particular for the DIP excess phase in the PFP:DIP 1:2 mixture, the size

of coherently scattering island l_s is by a factor of ∼4 smaller than in pure DIP films. In contrast, l_s of the PFP excess phase in the PFP:DIP 2:1 blend is not significantly reduced compared with pure PFP. Furthermore, also l_s of the intermixed crystal phase is influenced by the mixing ratio and is smallest in the PFP:DIP 1:2 blend. This indicates that the nucleation of the pure DIP phase is disturbed more easily by the simultaneous nucleation of the intermixed crystal phase and an excess DIP molecule is more probable to disturb the crystalline order of the mixed phase than an excess PFP molecule.

Independent of the mixing ratio, we observe pronounced changes in the line shape of $\epsilon_{2,\,xy}(E)$. By comparing the thickness regimes in which the structural and optical changes take place, we found strong indications that the evolutions in peak intensities in $\epsilon_{2,\,xy}(E)$ are resulting either from a reorientation of molecules or an increasing l_s, which is related to the structural order within the films. Our results illustrate the significant impact of the film structure on the optical properties in organic semiconductor blends and demonstrate the great potential of combined structural and optical real-time investigations.

ACKNOWLEDGMENTS

[1] W. Brütting and C. Adachi, *Physics of Organic Semiconductors* (Wiley VCH-Verlag, Weinheim, 2012).
[2] M. Bendikov, F. Wudl, and D. F. Perepichka, Chem. Rev. **104**, 4891 (2004).
[3] G. Witte and C. Wöll, J. Mater. Res. **19**, 1889 (2004).
[4] J. E. Anthony, Chem. Rev. **106**, 5028 (2006).
[5] S. R. Forrest, Nature (London) **428**, 911 (2004).
[6] F. Schreiber, Phys. Status Solidi A **201**, 1037 (2004).
[7] T. W. Kelley, P. F. Baude, C. Gerlach, D. E. Ender, D. Muyres, M. A. Haase, D. E. Vogel, and S. D. Theiss, Chem. Mater. **16**, 4413 (2004).
[8] N. Koch, ChemPhysChem **8**, 1438 (2007).
[9] J. Lewis, Mater. Today **9**, 38 (2006).
[10] J. O. Vogel, I. Salzmann, S. Duhm, M. Oehzelt, J. P. Rabe, and N. Koch, J. Mater. Chem. **20**, 4055 (2010).
[11] A. Aufderheide, K. Broch, J. Novák, A. Hinderhofer, R. Nervo, A. Gerlach, R. Banerjee, and F. Schreiber, Phys. Rev. Lett. **109**, 156102 (2012).
[12] R. Hesse, W. Hofberger, and H. Bässler, Chem. Phys. **49**, 201 (1980).
[13] A. Opitz, J. Wagner, W. Brütting, A. Hinderhofer, and F. Schreiber, Phys. Status Solidi A **206**, 2683 (2009).
[14] T. Sakurai, R. Fukasawa, K. Saito, and K. Akimoto, Org. Electron. **8**, 702 (2007).
[15] Y. Yoshida, H. Takiguchi, T. Hanada, N. Tanigaki, E.-M. Han, and K. Yase, J. Cryst. Growth **198–199**, 923 (1999).
[16] S. Heutz, P. Sullivan, B. Sanderson, S. M. Schultes, and T. S. Jones, Sol. Energy Mater. Sol. Cells **83**, 229 (2004).
[17] F. Würthner, C.-C. You, and C. R. Saha-Müller, Chem. Soc. Rev. **33**, 133 (2004).
[18] M. Campione, L. Raimondo, M. Moret, P. Campiglio, E. Fumagalli, and A. Sassella, Chem. Mater. **21**, 4859 (2009).
[19] L. Raimondo, M. Moret, M. Campione, A. Borghesi, and A. Sassella, J. Phys. Chem. C **115**, 5880 (2011).
[20] U. Heinemeyer, K. Broch, A. Hinderhofer, M. Kytka, R. Scholz, A. Gerlach, and F. Schreiber, Phys. Rev. Lett. **104**, 257401 (2010).
[21] M. Campione, A. Borghesi, M. Laicini, A. Sassella, C. Goletti, G. Bussetti, and P. Chiaradia, J. Chem. Phys. **127**, 244703 (2007).
[22] T. Hosokai, A. Gerlach, A. Hinderhofer, C. Frank, G. Ligorio, U. Heinemeyer, A. Vorobiev, and F. Schreiber, Appl. Phys. Lett. **97**, 063301 (2010).

[23] T. Dienel, R. Forker, K. Leo, and T. Fritz, J. Phys. Chem. C **111**, 14593 (2007).
[24] A. Sassella, A. Borghesia, M. Campione, L. Raimondo, C. Goletti, G. Bussetti, and P. Chiaradia, Superlattices Microstruct. **44**, 550 (2008).
[25] K. Broch, A. Aufderheide, L. Raimondo, A. Sassella, A. Gerlach, and F. Schreiber, J. Phys. Chem. C **117**, 13952 (2013).
[26] K. Broch, U. Heinemeyer, A. Hinderhofer, F. Anger, R. Scholz, A. Gerlach, and F. Schreiber, Phys. Rev. B **83**, 245307 (2011).
[27] F. Anger, J. O. Ossó, U. Heinemeyer, K. Broch, R. Scholz, A. Gerlach, and F. Schreiber, J. Chem. Phys. **136**, 054701 (2012).
[28] I. Salzmann, G. Heimel, S. Duhm, M. Oehzelt, P. Pingel, B. George, A. Schnegg, K. Lips, R.-P. Blum, A. Vollmer, and N. Koch, Phys. Rev. Lett. **108**, 035502 (2012).
[29] D. Beljonne, H. Yamagata, J. L. Brédas, F. C. Spano, and Y. Olivier, Phys. Rev. Lett. **110**, 226402 (2013).
[30] D. Datta, V. Tripathi, P. Gogoi, S. Banerjee, and S. Kumar, Thin Solid Films **516**, 7237 (2008).
[31] J.-L. Brédas, D. Beljonne, V. Coropceanu, and J. Cornil, Chem. Rev. **104**, 4971 (2004).
[32] J. P. Reinhardt, A. Hinderhofer, K. Broch, U. Heinemeyer, S. Kowarik, A. Vorobiev, A. Gerlach, and F. Schreiber, J. Phys. Chem. C **116**, 10917 (2012).
[33] J. Wagner, M. Gruber, A. Hinderhofer, A. Wilke, B. Bröker, J. Frisch, P. Amsalem, A. Vollmer, A. Opitz, N. Koch, F. Schreiber, and W. Brütting, Adv. Funct. Mater. **20**, 4295 (2010).
[34] A. C. Dürr, F. Schreiber, M. Münch, N. Karl, B. Krause, V. Kruppa, and H. Dosch, Appl. Phys. Lett. **81**, 2276 (2002).
[35] N. Karl, K. H. Kraft, J. Marktanner, M. Münch, F. Schatz, R. Stehle, and H.-M. Uhde, J. Vac. Sci. Technol. A **17**, 2318 (1999).
[36] M. Scharnberg, R. Adelung, and F. Faupel, Phys. Status Solidi A **205**, 578 (2008).
[37] T. Breuer and G. Witte, Phys. Rev. B **83**, 155428 (2011).
[38] J. Götzen, C. H. Schwalb, C. Schmidt, G. Mette, M. Marks, U. Höfer, and G. Witte, Langmuir **27**, 993 (2011).
[39] A. Hinderhofer, U. Heinemeyer, A. Gerlach, S. Kowarik, R. M. J. Jacobs, Y. Sakamoto, T. Suzuki, and F. Schreiber, J. Chem. Phys. **127**, 194705 (2007).
[40] T. Breuer, M. A. Celik, P. Jakob, R. Tonner, and G. Witte, J. Phys. Chem. C **116**, 14491 (2012).
[41] C. Schmidt, T. Breuer, S. Wippermann, W. G. Schmidt, and G. Witte, J. Phys. Chem. C **116**, 24098 (2012).
[42] I. Salzmann, S. Duhm, G. Heimel, J. P. Rabe, N. Koch, M. Oehzelt, Y. Sakamoto, and T. Suzuki, Langmuir **24**, 7294 (2008).
[43] Y. Sakamoto, T. Suzuki, M. Kobayashi, Y. Gao, Y. Fukai, Y. Inoue, F. Sato, and S. Tokito, J. Am. Chem. Soc. **126**, 8138 (2004).
[44] A. Hinderhofer and F. Schreiber, ChemPhysChem **13**, 628 (2012).
[45] A. Hinderhofer, C. Frank, T. Hosokai, A. Resta, A. Gerlach, and F. Schreiber, J. Chem. Phys. **134**, 104702 (2011).
[46] H. Proehl, R. Nitsche, T. Dienel, K. Leo, and T. Fritz, Phys. Rev. B **71**, 165207 (2005).
[47] R. Forker, M. Gruenewald, and T. Fritz, Annu. Rep. Prog. Chem., Sect. C: Phys. Chem. **108**, 34 (2012).
[48] R. Forker and T. Fritz, Phys. Chem. Chem. Phys. **11**, 2142 (2009).
[49] B. Krause, F. Schreiber, H. Dosch, A. Pimpinelli, and O. H. Seeck, Europhys. Lett. **65**, 372 (2004).
[50] S. Kowarik, A. Gerlach, S. Sellner, F. Schreiber, L. Cavalcanti, and O. Konovalov, Phys. Rev. Lett. **96**, 125504 (2006).
[51] A. Amassian, V. A. Pozdin, T. Desai, S. Hong, A. Woll, J. Ferguson, J. Brock, G. Malliaras, and J. Engstrom, J. Mater. Chem. **19**, 5580 (2009).
[52] S. Hong, A. Amassian, A. R. Woll, S. Bhargava, J. D. Ferguson, G. G. Malliaras, J. D. Brock, and J. R. Engstrom, Appl. Phys. Lett. **92**, 253304 (2008).
[53] R. Banerjee, J. Novák, C. Frank, C. Lorch, A. Hinderhofer, A. Gerlach, and F. Schreiber, Phys. Rev. Lett. **110**, 185506 (2013).
[54] B. Patterson, R. Abela, H. Auderset, Q. Chen, F. Fauth, F. Gozzo, G. Ingold, H. Kühne, M. Lange, D. Maden, D. Meister, P. Pattison, T. Schmidt, B. Schmitt, C. Schulze-Briese, M. Shi, M. Stampanoni, and P. Willmott, Nucl. Instrum. Methods Phys. Res. A **540**, 42 (2005).
[55] P. Willmott, D. Meister, S. Leake, M. Lange, A. Bergamaschi, M. Boege, M. Calvi, C. Cancellieri, N. Casati, A. Cervellino *et al.*, J. Synchrotron Rad. **20**, 667 (2013).
[56] M. Björck and G. Andersson, J. Appl. Crystallogr. **40**, 1174 (2007).
[57] L. G. Parratt, Phys. Rev. **95**, 359 (1954).
[58] S. Kowarik, A. Gerlach, S. Sellner, L. Cavalcanti, O. Konovalov, and F. Schreiber, Appl. Phys. A: Mater. Sci. Process. **95**, 233 (2009).

[59] M. Wojdyr, J. Appl. Crystallogr. **43**, 1126 (2010).
[60] M. Birkholz, *Thin Film Analysis by X-Ray Scattering* (Wiley-VCH, Weinheim, 2006).
[61] We note that for all blends considered here the crystallite sizes are much smaller than typical island sizes as determined using atomic force microscopy. Therefore, grain boundaries strongly contribute to disorder and defects in the film.

[62] Y. Wakayama, D. G. de Oteyza, J. M. Garcia-Lastra, and D. J. Mowbray, ACS Nano **5**, 581 (2011).
[63] H. Proehl, T. Dienel, R. Nitsche, and T. Fritz, Phys. Rev. Lett. **93**, 097403 (2004).
[64] U. Heinemeyer, R. Scholz, L. Gisslén, M. I. Alonso, J. O. Ossó, M. Garriga, A. Hinderhofer, M. Kytka, S. Kowarik, A. Gerlach, and F. Schreiber, Phys. Rev. B **78**, 085210 (2008).